ACS APPLIED MATERIALS & INTERFACES

Research Article

www.acsami.org

Steering the Efficiency of Carbon Nanotube–Silicon Photovoltaic Cells by Acid Vapor Exposure: A Real-Time Spectroscopic Tracking

C. Pintossi,[†] S. Pagliara,[†] G. Drera,[†] F. De Nicola,[‡,§] P. Castrucci,[‡,§] M. De Crescenzi,[‡,§] M. Crivellari,[∥] M. Boscardin,[∥] and L. Sangaletti*[,†]

[†]Interdisciplinary Laboratories for Advanced Materials Physics (I-LAMP) and Dipartimento di Matematica e Fisica, Università Cattolica del Sacro Cuore, I-25121 Brescia, Italy

[‡]Dipartimento di Fisica, Università degli Studi di Roma Tor Vergata, I-00133 Rome, Italy

[§]Istituto Nazionale di Fisica Nucleare, Università di Roma Tor Vergata (INFN-Roma Tor Vergata), I-00133, Rome, Italy

[∥]Fondazione Bruno Kessler, I-38100 Trento, Italy

Supporting Information

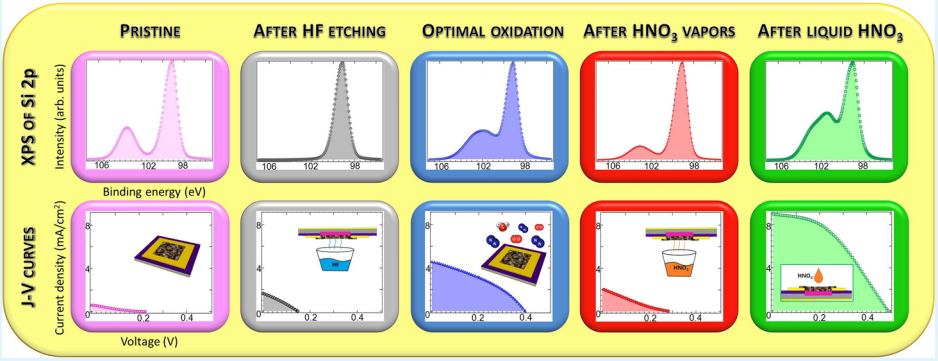

ABSTRACT: Hybrid carbon nanotube-silicon (CNT–Si) junctions have been investigated by angle resolved photoemission spectroscopy (AR-XPS) with the aim to clarify the effects of a nonstoichiometric silicon oxide buried interface on the overall cell efficiency. A complex silicon oxide interface has been clearly identified and its origin and role in the heterojunction have been probed by exposing the cells to hydrofluoric (HF) and nitric (HNO_3) acid. Real-time monitoring of the cell efficiencies during the steps following acid exposure (up to 1 week after etching) revealed a correlation between the thickness and chemical state of the oxide layer and the cell efficiencies. By matching the AR-XPS and Raman spectroscopy with the electrical response data it has been possible to discriminate the effects on the cell efficiency of the buried SiO_x interface from those related to CNT acid doping. The overall cell behavior recorded for different thicknesses of the SiO_x interface indicates that the buried oxide layer is likely acting as a passivating/inversion layer in a metal–insulator-semiconductor junction.

KEYWORDS: *carbon nanotubes, photovoltaics, CNT–Si hybrid junctions, photoemission, Raman spectroscopy, J–V characteristics*

INTRODUCTION

Hybrid devices based on heterojunctions between carbon nanotubes (CNTs) and silicon are among the most promising alternatives to silicon photovoltaics (PV) because of the remarkable power conversion efficiencies (PCE or η) so far displayed by devices based on these junctions.[1,2] The high efficiency reported for these systems is related to the peculiar physical properties of CNTs. On one side, single-walled carbon nanotubes (SWCNT) are excellent candidates for participating in photogeneration processes, because of their capability of absorbing light over a wide range of the solar spectrum, thanks to an energy bandgap variable from 0 to 3 eV, depending on the tube diameter, and to the presence in their density of states (DOS) of characteristic van Hove singularities. On the other side, it has been recently proved[3] that SWCNTs do not merely act as a light absorber layer but, due to their extraordinary electrical conductivity ($\sim 10^6$ S/cm),[4] they are also able to provide efficient transport paths for carriers, which have a very high probability to reach electrodes and generate photocurrent in devices based on CNTs photoexcitation processes.[5]

A considerable effort has been recently made to increase the efficiency of CNT–Si heterojunctions, until reaching a record PCE of about 15%.[6] However, much has still to be done in order to identify the mechanisms behind the device operation and determine the parameters that mostly affect the cell behavior. In addition to a number of technical issues related to the cell geometry, to contacting pads, and to the choice of the CNT layer, several studies have pointed out[2,7,8] that a silicon

Received: December 19, 2014
Accepted: April 22, 2015
Published: April 22, 2015

DOI: 10.1021/am508973b
ACS Appl. Mater. Interfaces 2015, 7, 9436–9444

oxide layer grows at the interface between monocrystalline silicon and CNTs not only during the manufacturing process but also once the junction is built and that the properties of this layer may affect the overall cell performances.

The role played by the oxide layer is of fundamental importance for understanding the working mechanism behind these devices that could behave either as p−n junctions[9] or as a metal−insulator−semiconductor (MIS) devices.[10] In particular, in a p−n junction model, the best efficiency should be reached once all the insulating silicon oxides are removed and perfect junctions between CNTs and Si can be built. On the other hand, in MIS junctions a relatively low potential barrier between CNTs and silicon yields a high number of majority carriers recombinations, resulting in a saturation current larger than that of a p−n junction diode and, as a consequence, in a low open circuit voltage. In these devices a thin layer of insulating oxide is beneficial because it helps to confine electrons in silicon, avoiding them to fast recombine in CNTs.[11] Moreover, a thin insulating layer may also have the advantage to passivate interface states, hindering charge trapping, lowering recombinations and increasing the device open circuit voltage.

The choice between the two junction schemes (i.e., p−n vs MIS) is still an open question that requires a specific investigation on the oxide role through direct evidence of the Si oxidation states during all the etching and aging processes aimed to tailor the oxide layer properties.

Oxide removal from silicon upon HF exposure is expected, as it is a standard treatment to etch silicon wafers and, on this basis, similar results have been claimed when CNT/Si heteojunctions were HF etched.[8,12] However, the results of the treatment are not usually documented by a probe sensitive to the Si oxidation state.

The possibility to access the buried interface layer by angle resolved X-ray photoemission spectroscopy (AR-XPS) has recently been demonstrated on devices similar to those analyzed in the present work.[13] Though the existence of an oxide layer with optimal thickness was inferred by several groups[7,8,13] to rationalize the behavior of the cells in the presence or absence of oxides, a complete analysis of this layer was so far overlooked and a direct evidence of the optimal layer thickness and composition is still virtually missing. Therefore, in spite of a seemingly straightforward preparation route, the CNT/SiO_x/Si interface represents a quite complex system from the point of view of materials, as it matches a relatively low-density CNT bundle layer with a nanostructured and chemically inhomogeneous SiO_x layer grown on a *n*-doped silicon wafer.

In particular, in devices based on bundles of randomly aligned SWCNTs the presence of a thin layer of oxides has always lead to better cell performances.[7,8,13] As shown by Jia et al.,[7] the electrical parameters of a CNT/Si solar cell can be modulated by changing the thickness of the SiO_x layer, either by removing oxides with HF or by letting these oxides regrow, through either oxidation in ambient air or exposure to HNO_3. Since now, several groups[7,8] have used exposure to HNO_3 to grow silicon oxides as a rapid alternative to ambient air oxidation, treating the two methods as if they would lead to equivalent results. On the other hand, it is also well established that HNO_3 can be used to further p-dope the CNTs,[14−17] disclosing the possibility that HNO_3 does not merely act as an oxidant agent, but also as a chemical dopant. The 2-fold role of HNO_3 must be clarified and silicon oxidation and CNT doping processes need to be analyzed and discussed separately, with the help of suitable experimental techniques.

Moreover, it is worth noting that efficient control of Si passivation through the introduction of a uniform and dense SiO_x layer is crucial to reduce leakage currents and to suppress charge recombination, in metal-oxide-semiconductor (MOS) devices, as shown by Kobayashi et al.[18] by considering nitric acid oxidation of silicon in conventional all-Si solar cells, as well as in Si/organic hybrid solar cells.[19]

It is clear that a deeper understanding of the role played by acids in modifying the properties of CNTs, Si and SiO_x is mandatory. This can be accomplished by directly probing the changes of the physical and chemical properties of the surface and the buried interface through suitable spectroscopic tools.

The purpose of the present work is then (i) to directly show on the device to which extent and how the hydrofluoric and nitric acid treatments affect the physical properties of both CNTs and the buried SiO_x interface and (ii) to probe how the CNT doping induced by HNO_3 exposure affects the overall cell behavior, discriminating effects on the CNT bundle layer from those due to changes in the physicochemical properties of the oxide layer.

To achieve these goals, a combination of spectroscopic tools has been considered: AR-XPS for a direct probe of the buried oxide interface, Raman spectroscopy to obtain information on CNT properties, and the acquisition of current density−voltage ($J-V$) characteristics for monitoring the behavior of the photovoltaic device after exposure to acid. These techniques have been applied to the different steps of oxidation or acid exposure in order to obtain a real-time monitoring of the chemical and physical properties of the interface. Within this experimental frame, the HF etching resulted to be crucial to restore a common starting point between the samples in terms of interface oxide removal, directly and nondestructively documented by XPS analysis.

It is worth mentioning that our HF treatments were milder than those carried out by Li et al.[12] that were able to n-dope their SWNTs after a 5 min exposure to HF vapors. In this way it was possible to explore a junction between n-type CNT layer and a p-type silicon substrate, which is a reversed scheme with respect to the one discussed in the present study (p-type CNT layer onto n-type Si wafer).

While in a previous paper,[13] the study of HF etching by AR-XPS analysis was reported basically at a feasibility stage, here we fully exploit this approach to address several problems, spanning from the effects of HF etching to those of HNO_3 treatments and the tracking of spontaneous oxidation in air. This breadth of phenomena will be addressed by a combined spectroscopy study that goes beyond the usual characterization tools (transmission spectroscopy and sheet resistance measurements) aimed to monitor the effects of acid treatments.

On the basis of this experimental approach, a clear correlation between the measured buried oxide layer thickness and the cell efficiency is demonstrated. Furthermore, the silicon oxide stoichiometry is also found to significantly affect the cell behavior. Finally, we have been able to show that, in the Si−CNT junction, HNO_3 behaves both as silicon oxidizing agent and a source of CNT chemical doping.

MATERIALS AND METHODS

SWCNT/Si PV Devices Fabrication. In this study, two PV cells, hereafter labeled A and B, were considered. The devices were realized by vacuum filtrating, respectively, 2 and 4 mL of semiconducting (7,6)

DOI: 10.1021/am508973b
ACS Appl. Mater. Interfaces 2015, 7, 9436−9444

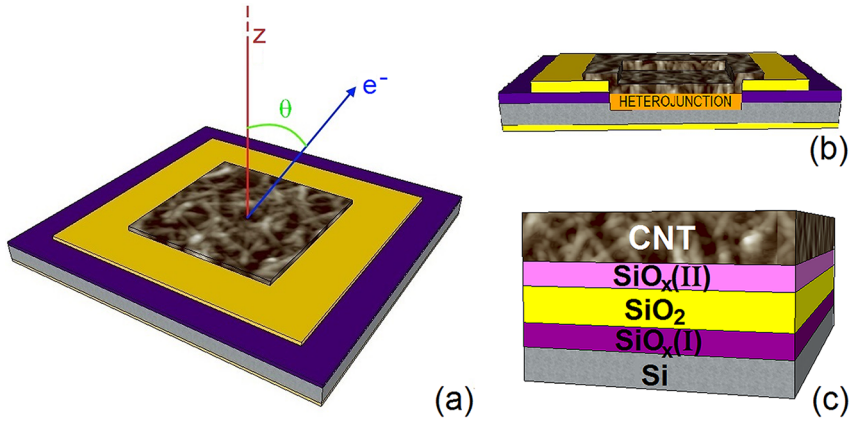

Figure 1. Three-dimensional sketch (a) and cross section (b) views of the CNT−Si hybrid photovoltaic device. (c) Model of the complex buried interface as a stack of (bottom to top layer) $Si/SiO_x(I)/SiO_2/SiO_x(II)/CNT$ layers.

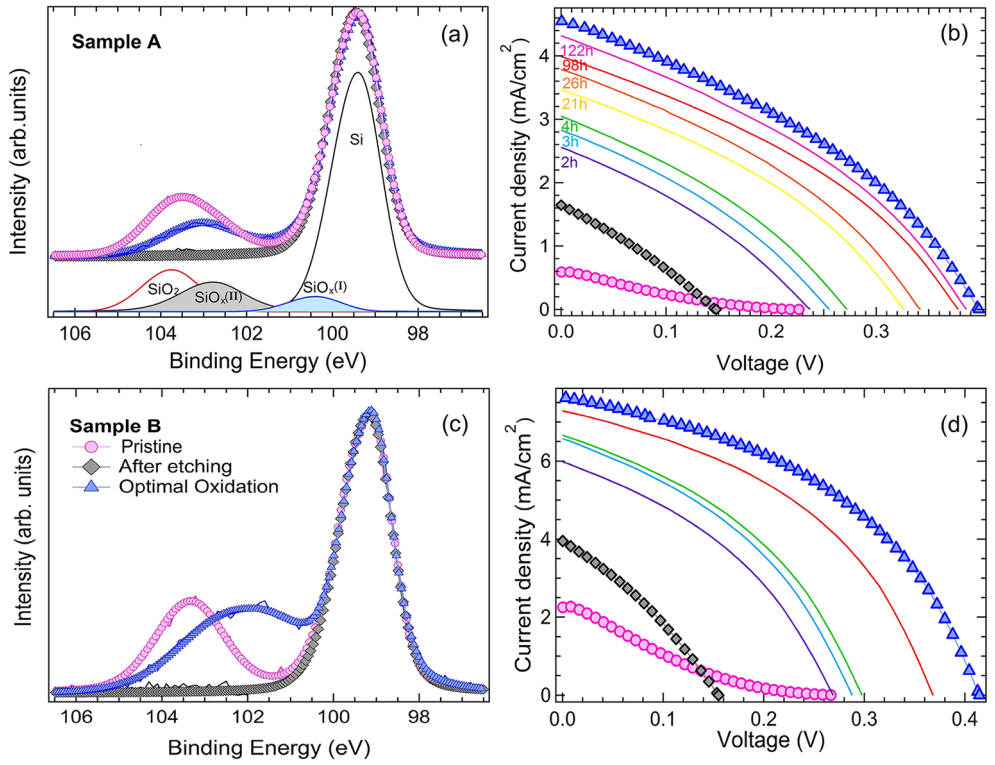

Figure 2. Si 2p XPS spectra for sample A (a) and sample B (c) and $J-V$ characteristic for sample A (b) and B (d) at different oxidation stages: pristine (pink circles), after HF etching (black diamonds) and at optimal oxidation (blue triangle). In panel a, the four Voigt subpeaks which fit the Si 2p core lines of the pristine sample A are also shown. In panels b and d, the $J-V$ curves measured in the time lag between HF etching and the optimal oxidation state are also shown (thin lines).

SWCNT solution on a cellulose filter, later removed in acetone, following the same manufacturing process described in refs 13 and 20 resulting in a final CNT film thickness of (26.2 ± 0.8) nm and (31.4 ± 0.9) nm, respectively (CNT film thicknesses obtained through the AR-XPS analysis, see Supporting Information and ref 13). The substrates are based on a 1 × 1 cm^2 slice of n-type Si(100) (resistivity 3−12 Ω·cm), passivated with 300 nm of SiO_2, covered by Cr/Au front electrode in which a window of 3 × 3 mm^2 has been obtained by lithographic processes. A Cr/Au ohmic contact was finally realized on the backside of the sample. The layout of the device is shown in Figure 1a, while a cross section and the model stack of layers across the Si-CNT junction are shown in Figure 1b and c, respectively.

Experimental Setup. XPS spectra were collected at a base pressure of 2 × 10^{-10} mbar by using the Al K_α line ($h\nu$ = 1486.6 eV, resolution 0.85 eV) from a twin anode (Al K_α and Mg K_α) X-ray source and a VG-Scienta R3000 spectrometer, calibrated following the procedure described in ref 21. Raman spectra were collected with a Renishaw spectrometer equipped with a He−Ne laser (λ = 632.8 nm) and a Leika confocal microscope. A 50× microscope objective (NA = 0.75) was used, with a laser power on the sample of about 1.4 mW. Electrical responses were collected with a halogen lamp (irradiance 64 mW/cm^2) and a custom-made $J-V$ tracker, driven by a National Instrument PCIe-6251 data acquisition board through the labVIEW software package.

RESULTS AND DISCUSSION

Effects of Exposure to HF. As devices were prepared in air, before starting any exposure to HF or HNO_3 it was necessary to record the initial cell efficiency through the

DOI: 10.1021/am508973b
ACS Appl. Mater. Interfaces 2015, 7, 9436−9444

Table 1. Electrical Characteristics (η, FF) and Estimated Layer Thicknesses of Sample A[a]

	η (%)	FF (%)	CNT (nm)	SiO_x(II) (nm)	SiO_2 (nm)	SiO_x(I) (nm)	total (nm)
pristine	0.035	18.93	26.20	0.47	0.73	0.28	1.48
after HF	0.107	28.96	26.20			0.35	0.35
optimal oxidation	1.012	35.45	26.20	0.20	0.60	0.65	1.45

[a]Thickness values in silicon oxide layers are given with a ±0.05 nm error.

Table 2. Electrical Characteristics (η, FF) and Estimated Layer Thicknesses of Sample B[a]

	η (%)	FF (%)	CNT (nm)	SiO_x(II) (nm)	SiO_2 (nm)	SiO_x(I) (nm)	total (nm)
pristine	0.147	17.91	31.41	0.24	1.72	0.55	2.51
after HF	0.295	31.88	31.41			0.64	0.64
optimal oxidation	2.297	48.28	31.41	0.72	1.23	0.36	2.31

[a]Thickness values in silicon oxide layers are given with a ±0.05 nm error.

acquisition of J-V curves on the pristine samples and to probe the silicon oxidation state with XPS at the pristine CNT−Si heterojunction (pink circles in Figure 2). Incidentally, it is worth mentioning that the *starting* efficiency of our solar cells (0.035% and 0.147%, for samples A and B, respectively) are low if compared to those recently reported in literature.[6,7,10,15] The cells were not optimized to yield the highest efficiencies, as the main focus was the detection of relative changes upon acid exposure. To access the SiO_x buried interface by AR-XPS, the CNT layer thickness is chosen to be relatively low. A similar choice was also made by, for example, Tune et al.,[8] that selected the devices not on the basis of their performances but, in that case, to guarantee the reproducibility of results.

Moreover, these relatively low efficiencies are also determined by our experimental setup (halogen lamp, irradiance 64 mW/cm^2) which differs from the standard ones (solar simulator, 100 mW/cm^2) both in terms of power and spectral composition. However, this point would not affect the validity of our analysis, since we were looking for changes in the efficiency and in the electrical cell behavior by comparing different oxidation and doping states of the same sample.

XPS survey spectra collected on the pristine samples showed the presence of C, Si, and O, along with Na that was ascribed to traces of the CNT solution surfactant.

High-resolution XPS studies on the Si oxidation,[22−25] have shown that many oxide species can be detected during the oxidation process, each characterized by a specific binding energy (BE). In addition to bulk silicon (Si^0) the core lines of three suboxides (Si^{1+}, Si^{2+}, Si^{3+}) can be found in the binding energy range between Si and SiO_2. Even though our experimental resolution was lower than the one reached by using synchrotron radiation,[22] we needed at least four peaks (Voigt functions) to correctly fit the Si 2p XPS spectra. These peaks ranged from BE = 99.1 eV for bulk silicon to BE = 102.9 eV for SiO_2 with two additional peaks ascribed to non-stoichiometric silicon oxides. This choice was made necessary in particular for correctly fitting the Si 2p peak after the HF etching, in which almost all the oxides were removed except for the Si^+ component, hereafter labeled as SiO_x(I), which determined an asymmetric line shape of the Si^0 peak (see Supporting Information, Figure S1 and related comments). Since our experimental resolution does not allow for the resolution of the Si^{2+} and Si^{3+} contributions, they have been fit to a single peak and labeled as SiO_x(II).

Then, performing AR-XPS by varying the photoelectron takeoff angle θ (Figure 1a), it was possible to evaluate the thickness of each layer composing our devices (Tables 1 and 2), following the method described in ref 13. Details of the data analysis approach are also provided in the Supporting Information (Figure S2 and related comments). Based on this analysis, the four peaks have been ascribed to (i) bulk silicon (BE = 99.1 eV), (ii) nonstoichiometric silicon oxide (SiO_x(I)) (BE = 99.7 eV), which grows as a very thin layer on Si that eventually turns into SiO_2 during silicon oxidation process,[22−25] (iii) stoichiometric SiO_2 (BE = 102.9 eV), and (iv) nonstoichiometric silicon oxide (SiO_x(II)) (BE = 101.3 eV), which lies between SiO_2 and the CNT layer, where oxygen atoms are likely shared between SiO_2 and the CNT bundles. The energetic preference for the CNT to bind on particular sites of an O-terminated SiO_2 surface has been predicted by M. Zubaer Hossain,[26] indicating a significant interaction between oxygen from the SiO_x layer with CNT.

The model stack of layers considered in the present study is depicted in Figure 1c.

After these characterizations, both samples were etched with HF vapors for 20 s to remove all silicon oxides, as confirmed by XPS analysis (Figure 2, black diamonds). Incidentally, we point out that our HF treatments have a different purpose as compared to those previously carried out by Li et al.[12] In that case, the etching was mainly addressed to remove oxygen from the tube walls and therefore to n-dope the CNTs, which in general are naturally p-doped in air due to O_2 adsorption. Therefore, a 5 min exposure in a vapor phase etcher was required to achieve n-doping. Then, samples had to be stored and analyzed into a nitrogen-filled glovebox to prevent nanotubes from coming into contact with oxygen, which would have p-doped the tubes again. On the other hand, our devices are based on p-doped CNTs so acid exposure and all measurements can be performed in air and a milder HF etching of 20 s is sufficient to remove silicon oxides without affecting the CNT doping.

Even if samples were stored in the UHV analysis chamber just after the HF etching and the collection of the $J-V$ curve, the time elapsed before reaching high vacuum conditions was enough to have the samples exposed to air and trigger the silicon oxidation. Indeed this process is known to be quite fast[23] and even just few minutes after etching the effects of oxidation are detectable, in the present case as a small shoulder on the high BE side of the Si 2p core level. As a result, even after the oxides removal, a small quantity of SiO_x(I) is detected (Figure 2a and c). After the XPS analysis of the HF etched samples, the devices were exposed to air and the effects of oxidation were tracked through the $J-V$ curves. The $J-V$ curves in Figure 2b and d clearly highlight poor cell performances also in device

DOI: 10.1021/am508973b
ACS Appl. Mater. Interfaces 2015, 7, 9436−9444

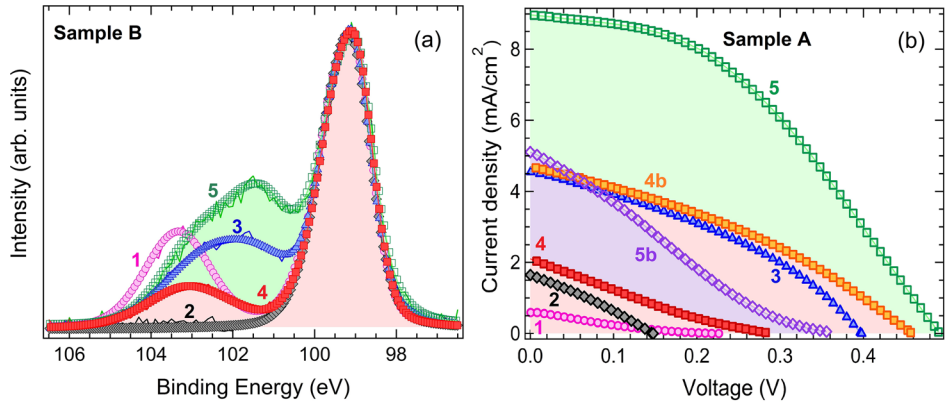

Figure 3. Si 2p X.-ray photoemission spectra measured for sample B (a) and $J-V$ characteristic curves measured for sample A (b) at different conditions determined by the PV cell treatment: (1) pink filled circles, pristine samples; (2) black filled diamonds, after HF etching; (3) blue filled triangles, optimal oxidation; (4) red filled squares, after exposure to HNO_3 vapors; (4b) orange filled squares, at the optimal oxidation state after exposure to HNO_3; (5) green empty squares, after soaking samples with HNO_3 drop; (5b) purple empty diamonds, after the HNO_3 drop drying.

without oxides (data collected immediately after the HF etching), but just after 2 h of oxidation in ambient air the efficiency starts to grow, following a rate (Supporting Information, Figures S3 and S4) very similar to the silicon oxidation rate at room temperature detected for silicon wafers, which is known to be quite fast in the first hours and then displaying a logarithmic-like growth rate).[23] Selected $J-V$ curves during the oxidation are shown in Figure 2b and d (thin lines), while the complete tracking of V_{OC}, J_{SC}, and η as a function of the oxidation time is shown in the Supporting Information (Figures S3 and S4).

About 1 week after HF etching (170 h), sample A and B reached their highest efficiency (1.01% and 2.30%, respectively), which is also assumed as the moment when the device has reached an optimal oxidation state (blue triangle in Figure 2). Through the AR-XPS analysis, we have been able for the first time to provide an estimation of the thickness of the silicon oxide layer yielding the best cell performances, as reported in Tables 1 and 2.

At this stage two conclusions can be drawn. If we focus on the paths that lead sample A and B to their optimal oxidation states starting from the HF etching, which is assumed as the reference starting point, in both samples, an approximately 4-fold enhancement of the overall oxide layer thickness [SiO_x(II) + SiO_2 + SiO_x(I)/SiO_x(I)] is observed.

Furthermore, even if the buried oxide layer thickness is comparable in the pristine and optimally oxidized samples, the chemical state of Si shows a clear change, as after optimal oxidation an increase of SiO_x and a reduction of SiO_2 is registered. On the other hand the lack of oxide (Figure 2, black diamonds) is detrimental to the performances of both cells, testifying an overall similar behavior.

These results induce to consider the oxide buried interface acting as a passivating/inversion layer in a MIS device. Oxides improve the cell performances by, on one side, avoiding trapping at silicon interface state and, on the other side, by reducing e−h pair recombination (see, e.g., ref 19 and refs. therein). This happens provided that silicon oxide thickness is kept below an optimal value, to prevent the detrimental effect of a large barrier to charge separation after the e−h pair is created and to the hole photocurrent flow toward the CNT film.

Referring to the Si−CNT hybrid cells, in principle, it should be easy to distinguish the two different junction models (i.e., p−n junction vs MIS). If the efficiency grows when silicon oxides are completely removed by HF, the device can be modeled by a p−n junction, while if the device works better with a thin layer of Si oxides, the most suitable model is the MIS stack of layers. In literature, however, the role of the oxide layer in CNT/Si PV devices is an open matter of dispute,[6−10,13,15,27,28] where the morphology of the CNT layer can play a relevant role. Evidence of devices working better with a thin layer of oxides (like MIS heterojunctions) are provided in the case of *randomly aligned* CNTs.[7,8,13] In fact, a perfect junction with silicon is hindered by the morphology of the CNT bundles, where only a few number of CNTs is effectively in contact with the crystalline silicon underneath. When the amorphous silicon oxide grows, a higher number of heterojunctions is built up and the device efficiency improves.

Finally, we noticed that $J-V$ curves yielded the same results when measured after up to five HF etchings (20 s each), at least. Additional etches in some cases led to the degradation of the electrical contacts removing the SiO_2 insulating layer under the electrical contacts and yielding shorts between the electrodes and the n-type Si wafer. In addition, the XPS data were comparable both in terms of successful SiO_x removal and in terms of the Na content, that was not affected by HF etching (while being affected by HNO_3 exposure, as shown in the next Subsection).

Effects of Exposure to HNO_3. As mentioned in the introductory remarks, HNO_3 exposure is also often regarded as a tool to induce silicon oxidation but it may also lead to further p-doping of the CNT layer. To understand what ultimately affects cell performances, it is mandatory to discriminate these two effects separately, using AR-XPS measurements, performed in UHV, to monitor silicon oxidation, and Raman spectroscopy, and $J-V$ characteristics, all performed in air, to highlight the eventual CNT doping. Since our two samples display a similar qualitative behavior, we resorted to analyze them separately, putting sample B in the UHV analysis chamber immediately after every acid treatment, to preserve it as much as possible from unwanted silicon oxidation occurring immediately after Si HF etching, and using sample A for the $J-V$ measurements performed in air.

Starting from the optimally oxidized samples, we restored a common initial condition by removing all oxides with HF (curves almost identical to those shown in Figure 2, black diamonds).

DOI: 10.1021/am508973b
ACS Appl. Mater. Interfaces 2015, 7, 9436−9444

Then, both samples were exposed to HNO_3 vapors at room temperature for 90 s, following the indications of ref 7. The effects of nitric acid exposure were monitored through AR-XPS analysis on sample B (Figure 3a) and through the J-V characteristics on sample A (Figure 3b).

Efficiencies and FFs for sample A are reported in Table 3, while the silicon oxides thicknesses for sample B are listed in Table 4. Immediately after the exposure to HNO_3, the device displays a slight increase of the efficiency (Table 3 and Figure 3b, curve 4 vs 2) but the oxidation state corresponding to the maximum η is reached only after leaving the device in air for 3 days (Table 3 and Figure 3, orange squares, curve 4b). As clearly shown by the Si 2p spectrum (curve 4, Figure 3a) and in the results of the AR-XPS analysis (Table 4), this indicates that the silicon oxidation immediately after HNO_3 exposure (curve 4, Figure 3a) is not sufficient to yield the optimal oxidation state. After oxidation in air (curve 4b, Figure 3b), the maximum η is now slightly higher than the one reached without HNO_3 exposure (curve 3, triangles, in Figure 3b), giving a first suggestion of possible CNT doping.

Table 3. η and FF of HNO_3 Treatments of sample A

	H (%)	FF (%)
HNO_3 vapors	0.197	20.52
optimal oxidation	1.163	34.29
HNO_3 liquid	2.866	41.69
after acid drying	0.651	22.99

Table 4. Thicknesses of Sample B Layers after HNO_3 Treatments[a]

	CNT (nm)	SiO_x(II) (nm)	SiO_2 (nm)	SiO_x(I) (nm)	total (nm)
HNO_3 vapors	31.41	0.29	0.83	0.52	1.64
HNO_3 liquid	31.41	0.79	1.54	1.18	3.51

[a]Thickness values in silicon oxide layers are given with a ±0.05 nm error.

Since, at the present experimental conditions (T = 20 °C, exposure time 90 s, acid dilution 65%) only a low number of HNO_3 molecules effectively come into contact with CNT and Si, the nitric acid effects should be enhanced either by longer exposures or by directly wetting the devices with liquid HNO_3. We resorted to follow the second strategy: both samples were etched again with HF and immediately after etching a single drop of diluted HNO_3 (65% RPE-ISO, Carlo Erba Reagents) was placed on the top of the CNT film.

The result of this last treatment (HNO_3 soaking) is a remarkable increase of the efficiency to 2.87%, two and a half times greater than the best value of 1.16% recorded with HNO_3 vapors (green empty squares in Figure 3, curve 5). However, as the HNO_3 solution drop dries, 2 h after the treatment, the cell performances are found to worsen considerably (purple empty diamonds in Figure 3b, curve 5b), indicating that the initial jump of the efficiency is not only attributable to CNT p-doping alone but it can also be due (i) to a lensing effect by the acid droplet that focuses light on CNT surface,[28] and (ii) to a formation of a temporary electrochemical cell between CNT and Si in the HNO_3 solution.[15] The rapid efficiency decrease from 2.87% to 0.65% recorded after the acid drying can be interpreted as an effect of the huge amount of silicon oxides, detrimental for the device operation, originated by the strong oxidizing properties of the HNO_3 drop as shown in Figure 3a (green empty squares, curve 5), which was previously dominated by the favorable lensing effect.

The conclusion we draw on this set of data is summarized in Figure 4 where a correlation between efficiency and oxide thickness is shown. The efficiency is measured on sample A, and not on sample B but in the two stages where the efficiency of both layers (η_A and η_B) was available the values measured for sample B were about 3 times the corresponding values for sample A (η_B/η_A = 0.295/0.107 after the first HF etching, η_B/η_A = 1.55/0.49 three months after the latest HNO_3 treatment).

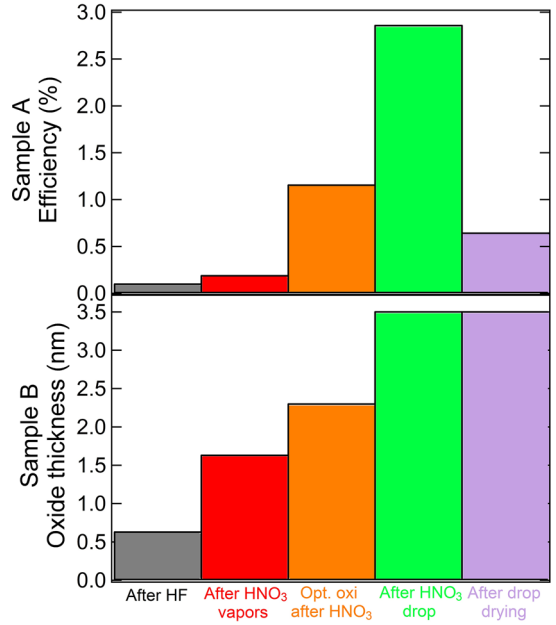

Figure 4. (Top panel) Efficiencies measured for sample A during various treatments of the cell. (Bottom panel) Overall oxide layer thickness for sample B.

The effects of HNO_3 on the photovoltaic device are also evident in the XPS survey spectra, normalized to the C 1s intensity (Figure 5a). In particular, before acid treatments, the percentage of oxygen present in the sample was 3.65%, which is almost doubled to 6.84% after exposure to HNO_3 vapors, and became five times higher after the soaking with HNO_3 drop, that is, 16.34% of the total probed area, indicating a clear oxidation induced by nitric acid. Furthermore, in all survey spectra, the Na 1s peak (as well as the Na Auger emission) ascribed to sodium dodecyl sulfate (SDS), the surfactant used to disperse the CNTs, resulted to be quenched by HNO_3, indicating a possible effect of surfactant removal.

Another interesting consequence of HNO_3 vapor exposure is the shift of the C 1s peak to lower BE (inset of Figure 5b). This shift, not observed after HF etching, is a clear indicator of a Fermi level shift due to a hole doping of nanotubes. In the case of the HNO_3 drop, the C 1s peak shifts to low BE but also changes its shape in the high BE region, indicating an increasing amount of oxygen bonded with the CNT carbon atoms.[29] These effects are more evident for the sample treated with liquid HNO_3, both because of the higher acid concentration and because HNO_3 in solution spends more time in contact with CNTs before evaporation, with respect to the gas phase.

DOI: 10.1021/am508973b
ACS Appl. Mater. Interfaces 2015, 7, 9436−9444

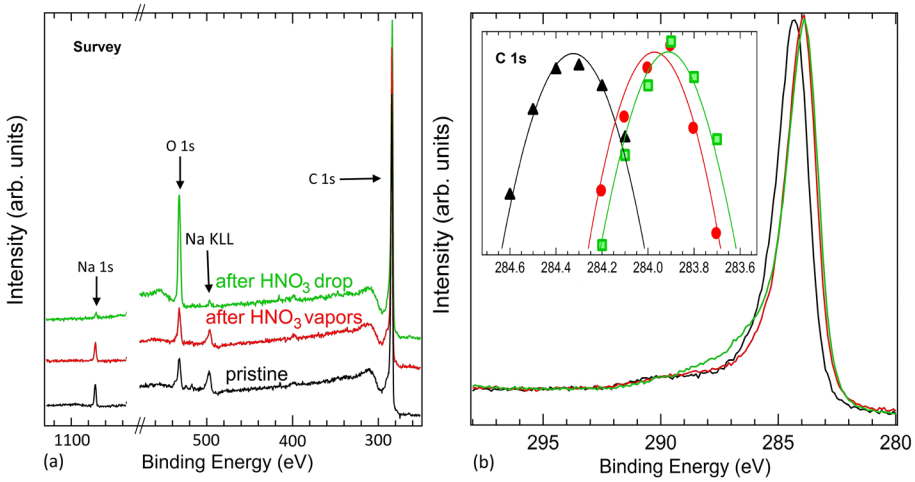

Figure 5. (a) Survey XPS spectra of sample B, normalized to the C 1s peak intensity. The C 1s, N 1s, and O 1s core levels are labeled, along with the Na Auger emission (b) C 1s spectra before and after acid treatment. Inset: Detail of the C 1s peak shift. Black line and triangles: Pristine sample. Red line and circles: After exposure to HNO_3 vapors. Green line and squares: After soaking with HNO_3 drop.

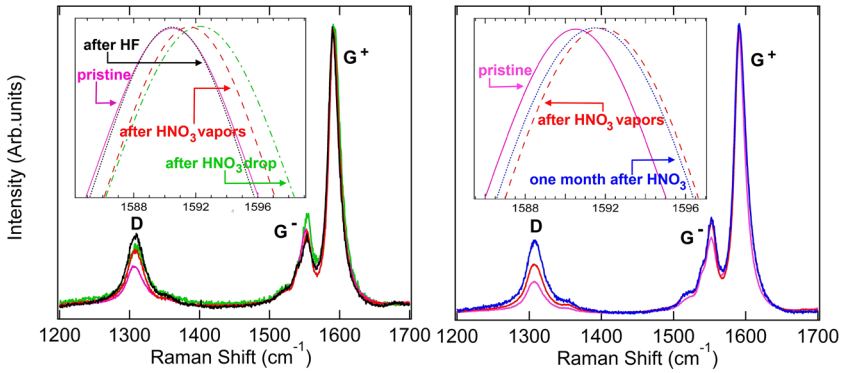

Figure 6. Raman spectra of D- and G-band of pristine (pink continuous line) sample A (left panel) and B (right panel), after HF (black dotted line), after HNO_3 vapors (red dashed curves), after HNO_3 drop (green dash-dotted line) and after one month from the acid treatments (blue dotted curve). The effect of HNO_3 doping is to shift the G^+ band toward higher Raman shifts as shown in the insets.

To unambiguously prove the CNTs doping effect, we also collected Raman spectroscopy and optical absorption data. In particular, Raman spectroscopy is suitable to study fundamental tube properties, such as chirality, purity and defects.[30] In particular, in the presence of hole doping, the G^+-band of semiconducting SWCNT was found to move about 1 cm^{-1} toward higher wavenumbers.[31] As shown in Figure 6 (left panel, sample A; right panel, sample B), while HF etching does not change the G^+-band position (1590.5 cm^{-1}), both gaseous and liquid HNO_3 exposures yield G^+ shifts of 0.9 and 1.8 cm^{-1}, respectively. This hole doping process is not completely reversible, because, even after a month in ambient air, sample B still presents a shift in the top of the G-band at 1591.4 cm^{-1}, which is less than the doped one (1592.3 cm^{-1}) but still far from the undoped value of 1590.5 cm^{-1}, as shown in Figure 6 (right panel). However, the CNT doping still observed 1 month after the HNO_3 exposure is not able to balance the detrimental effect on the cell efficiency of the thick oxide layer growth induced by the HNO_3 drop.

Optical spectroscopy data show, as expected,[32] a quenching of the S11 and S22 bands upon HNO_3 exposure (Supporting Information, Figure S5). These findings are also consistent with a decrease in the sheet resistance observed after HNO_3 exposure. Indeed, starting from a base resistance of 10674 ± 12 ohm, the sheet resistance drops to 2470 ± 4 ohm after 10 s exposure and to 1834 ± 7 ohm with an additional 10 s exposure.

CONCLUSION

In conclusion, a spectroscopic investigation of the hybrid CNT−Si heterojunctions has been carried out with the aim to find a correlation between the physical and chemical properties of a buried oxide interface and the device performances. To this purpose, *J*−*V* tracking curves after each treatment were collected, to be matched with spectroscopic data from AR-XPS and Raman probes. We have unambiguously demonstrated that, while a relatively mild HF etching does not change the CNT film properties, acting only as silicon oxides etcher, HNO_3 has the effect of both doping nanotubes and oxidizing the silicon underneath. This finding addresses a long-standing question on the CNT−Si hybrid junctions, probing the role of the complex silicon oxide interface to tailor the PV cell performances and discriminating the effects of oxidation and p-doping which occur upon exposure to HNO_3. While a further p-doping of CNT is suitable for reaching higher efficiency, HNO_3 (especially in its liquid form) has to be used carefully because its strong oxidizing effect is detrimental to the cell performances, as it may yield a thickness of the oxide layer above the value (1.5−2.0 nm) recorded for the best performances.

DOI: 10.1021/am508973b
ACS Appl. Mater. Interfaces 2015, 7, 9436−9444

HF etching was used to remove Si oxide from the buried interface. This helped us establish a common starting point before carrying out any of the treatments considered in the present study. The buildup of an interface Si oxide layer is required to increase the efficiency. This is assumed as a strong indication that the junction can be described with a MIS model rather than a p−n junction. HF treatment was not strong enough to n-dope the CNTs, as no change in the Raman and XPS spectra was observed upon HF exposure. HF etching did not affect the Na content of the CNT layer, unlike HNO_3 that was also able to etch Na away from the bundle layer.

The present results indicate that the SiO_x buried interface can be regarded as a passivating and inversion layer, which improves the cell performances by hindering the e−h pair recombination. Though these effects of the SiO_x interface in hybrid CNT−Si PV cells may have been unintentional in the original cell design, the thickness correlation with efficiency here demonstrated can provide a useful perspective in further device engineering.

■ ASSOCIATED CONTENT

Supporting Information

XPS Si 2p peak fit, evaluation of the oxide layers thickness from the analysis of AR-XPS data, tracking of the oxidation effects on the cell performances, effects of the HNO_3 treatment on the optical absorbance of CNTs, and references. The Supporting Information is available free of charge on the ACS Publications website at DOI: 10.1021/am508973b.

■ AUTHOR INFORMATION

Corresponding Author

*Phone: ++39-030-2406716. E-mail: sangalet@dmf.unicatt.it.

Author Contributions

The manuscript was written through contributions of all authors. All authors have given approval to the final version of the manuscript.

Notes

The authors declare no competing financial interest.

■ REFERENCES

(1) Tune, D. D.; Flavel, B. S.; Krupke, R.; Shapter, J. G. Carbon Nanotube−Silicon Solar Cells. *Adv. Energy Mater.* **2012**, *2*, 1043−1055.

(2) Castrucci, P. Carbon Nanotube/Silicon Hybrid Heterojunctions for Photovoltaic Devices. *Adv. Nano Res.* **2014**, *2*, 23−56.

(3) Tune, D. D.; Hennrich, F.; Dehm, S.; Klein, M. F. G.; Glaser, K.; Colsmann, A.; Shapter, J. G.; Lemmer, U.; Kappes, M. M.; Krupke, R.; Flavel, B. S. The Role of Nanotubes in Carbon Nanotube−Silicon Solar Cells. *Adv. Energy Mater.* **2013**, *3*, 1091−1097.

(4) Mc Euen, P. L.; Park, J. Y. Electron Transport in Single-Walled Carbon Nanotubes. *MRS Bull.* **2004**, *29*, 272−275.

(5) Ponzoni, S.; Galimberti, G.; Sangaletti, L.; Castrucci, P.; Del Gobbo, S.; Morbidoni, M.; Scarselli, M.; Pagliara, S. Selective Optical Switching of Interface-Coupled Relaxation Dynamics in Carbon Nanotube−Si Heterojunctions. *J. Phys. Chem. C* **2014**, *118*, 24110−24116.

(6) Shi, E.; Zhang, L.; Li, Z.; Li, P.; Shang, Y.; Jia, Y.; Wei, J.; Wang, K.; Zhu, H.; Wu, D.; Zhang, S.; Cao, A. TiO_2-Coated Carbon Nanotube-Silicon Solar Cells with Efficiency of 15%. *Sci. Rep.* **2012**, *2* (884), 1−5.

(7) Jia, Y.; Cao, A.; Kang, F.; Li, P.; Gui, X.; Zhang, L.; Shi, E.; Wei, J.; Wang, K.; Zhu, H.; Wu, D. Strong and Reversible Modulation of Carbon Nanotube-Silicon Heterojunctions Solar Cells by an Interfacial Oxide Layer. *Phys. Chem. Chem. Phys.* **2012**, *14*, 8391−8396.

(8) Tune, D. D.; Blanch, A. J.; Krupke, R.; Flavel, B. S.; Shapter, J. G. Nanotube Film Metallicity and its Effect on the Performance of Carbon Nanotube−Silicon Solar Cells. *Phys. Status Solidi A* **2014**, *211*, 1479−1487.

(9) Jung, Y.; Li, X.; Rajan, N. K.; Taylor, A. D.; Reed, M. A. Record High Efficiency Single-Walled Carbon Nanotube/Silicon p−n Junction Solar Cells. *Nano Lett.* **2013**, *13*, 96−99.

(10) Wadhwa, P.; Liu, B.; McCarthy, M. A.; Wu, Z.; Rinzler, A. G. Electronic Junction Control in a Nanotube-Semiconducting Schottky Junction Solar Cell. *Nano Lett.* **2010**, *10*, 5001−5005.

(11) Card, H. C. Photovoltaic Properties of MIS-Schottky Barriers. *Solid-State Electron.* **1977**, *20*, 971−976.

(12) Li, X.; Huang, J. S.; Nejati, S.; McMillon, L.; Huang, S.; Osuji, C. O.; Hazari, N.; Taylor, A. D. Role of HF in Oxygen Removal from Carbon Nanotubes: Implications for High Performance Carbon Electronics. *Nano Lett.* **2014**, *14*, 6179−6184.

(13) Pintossi, C.; Salvinelli, G.; Drera, G.; Pagliara, S.; Sangaletti, L.; Del Gobbo, S.; Morbidoni, M.; Scarselli, M.; De Crescenzi, M.; Castrucci, P. Direct Evidence of Chemically Inhomogeneous, Nanostructured, Si−O Buried Interfaces and Their Effect on the Efficiency of Carbon Nanotube/Si Photovoltaic Heterojunctions. *J. Phys. Chem. C* **2013**, *117*, 18688−18696.

(14) Lin, T.; Bajpai, V.; Ji, T.; Dai, L. Chemistry of Carbon Nanotubes. *Aust. J. Chem. Phys.* **2003**, *56*, 635−651.

(15) Jia, Y.; Cao, A.; Bai, X.; Li, Z.; Zhang, L.; Guo, N.; Wei, J.; Wang, K.; Zhu, H.; Wu, D.; Ajayan, P. M. Achieving High Efficiency Silicon−Carbon Nanotube Heterojunctions Solar Cells by Acid Doping. *Nano Lett.* **2011**, *11*, 1901−1095.

(16) Wang, F.; Kozawa, D.; Miyauchi, Y.; Hiraoka, K.; Mouri, S.; Matsuda, K. Enhancement Mechanism of the Photovoltaic Conversion Efficiency of Single-Walled Carbon Nanotube/Si Solar Cells by HNO_3 Doping. *Appl. Phys. Express* **2013**, *6* (102301), 1−4.

(17) Kamaras, K.; Pekker, A.; Botka, B.; Hu, H.; Niyogi, S.; Itkis, M. E.; Haddon, R. C. The Effect of Nitric Acid Doping on the Optical Properties of Carbon Nanotube Films. *Phys. Status Solidi B* **2010**, *247*, 2754−2757.

(18) Kobayashi, H.; Asuha; Maida, O.; Takahashi, M.; Iwasa, H. Nitric Acid Oxidation of Si to Form Ultrathin Silicon Dioxide Layers with a Low Leakage Current Density. *J. Appl. Phys.* **2003**, *94*, 7328−7335.

(19) Sheng, J.; Fan, K.; Wang, D.; Han, C.; Fang, J.; Gao, P.; Ye, J. Improvement of the SiO_x Passivation Layer for High-Efficiency Si/PEDOT:PSS Heterojunction Solar Cells. *ACS Appl. Mater. Interfaces* **2014**, *6*, 16027−16034.

(20) Del Gobbo, S.; Castrucci, P.; Fedele, S.; Riele, L.; Convertino, A.; Morbidoni, M.; De Nicola, F.; Scarselli, M.; Camilli, L.; De Crescenzi, M. Silicon Spectral Response Extension Through Single Wall Carbon Nanotubes in Hybrid Solar Cells. *J. Mater. Chem. C* **2013**, *1*, 6752−6758.

(21) Drera, G.; Salvinelli, G.; Åhlund, J.; Karlsson, P. G.; Wannberg, B.; Magnano, E.; Nappini, S.; Sangaletti, L. Transmission Function Calibration of an Angular Resolved Analyzer for X-ray Photoemission Spectroscopy: Theory vs Experiment. *J. Electron Spectrosc. Relat. Phenom.* **2014**, *195*, 109−116.

(22) Himpsel, F. J.; McFeely, F. R.; Taleb-Ibrahimi, A.; Yarmoff, J. A.; Hollinger, G. Microscopic Structure of the SiO_2/Si Interface. *Phys. Rev. B: Condens. Matter Mater. Phys.* **1988**, *38*, 6084−6096.

(23) Mende, G.; Finster, J.; Flamm, D.; Schulze, D. Oxidation of Etched Silicon in Air at Room Temperature: Measurements with Ultrasoft X-ray Photoelectron Spectroscopy (ESCA) and Neutron Activation Analysis. *Surf. Sci.* **1983**, *128*, 169−175.

(24) See, for example, Ohtsu, M., Ed. *Optical and Electronic Process of Nano-Matters*; Springer Science+Business Media: Dordrecht, the Netherlands, 2001; Chapter 10 and refs therein.

(25) Hollinger, G.; Himpsel, F. J. Probing the Transition Layer at the SiO_2−Si Interface Using Core Level Photoemission. *Appl. Phys. Lett.* **1984**, *44*, 93−95.

DOI: 10.1021/am508973b
ACS Appl. Mater. Interfaces 2015, 7, 9436−9444

(26) Zubaer Hossain, M. Interface Induced Band Gap Reduction and Electron Transfer in Semiconducting Carbon Nanotube. *Appl. Phys. Lett.* **2010**, *96*, No. 053118.
(27) Di, J.; Yong, Z.; Zheng, X.; Sun, B.; Li, B. Aligned Carbon Nanotubes for High Efficiency Schottky Solar Cells. *Small* **2013**, *9*, 1367−1372.
(28) Li, X.; Jung, Y.; Sakimoto, K.; Goh, T. H.; Reed, M. A.; Taylor, A. D. Improved Efficiency of Smooth and Aligned Single Walled Carbon Nanotube/Silicon Hybrid Solar Cells. *Energy Environ. Sci.* **2013**, *6*, 879−887.
(29) Wepasnick, K. A.; Smith, B. A.; Bitter, J. L.; Fairbrother, D. H. Chemical and Structural Characterization of Carbon Nanotube Surfaces. *Anal. Bioanal. Chem.* **2010**, *369*, 1003−1014.
(30) Dresselhaus, M. S.; Dresselhaus, G.; Saito, R.; Jorio, A. Raman Spectroscopy of Carbon Nanotubes. *Phys. Rep.* **2005**, *409*, 47−99.
(31) Zhou, W.; Vavro, J.; Nemes, N. M.; Fischer, J. E.; Borondics, F.; Kamarás, K.; Tanner, D. B. Charge Transfer and Fermi Level Shift in p-Doped Single-Walled Carbon Nanotubes. *Phys. Rev. B: Condens. Matter Mater. Phys.* **2005**, *71*, No. 205423.
(32) Ong, P. L.; Euler, W. B.; Levitsky, I. A. Hybrid Solar Cells Based on Single-Walled Carbon Nanotubes/Si Heterojunctions. *Nanotechnology* **2010**, *21*, No. 105203.

DOI: 10.1021/am508973b
ACS Appl. Mater. Interfaces 2015, 7, 9436−9444